Absorption spectroscopy of a radiatively heated samarium plasma

H. Merdji,[1] T. Mißalla,[1] T. Blenski,[1] F. Perrot,[2] J. C. Gauthier,[1] K. Eidmann,[3] and C. Chenais-Popovics[1]
[1]*Laboratoire pour l'Utilisation des Lasers Intenses, Centre National de la Recherche Scientifique, Ecole Polytechnique, 91128 Palaiseau Cedex, France*
[2]*CEA Limeil-Valenton, 94195 Villeneuve Saint-Georges Cedex, France*
[3]*Max-Planck-Institut für Quantenoptik, 85748 Garching, Germany*
(Received 2 September 1997)

We present measurements of the samarium ($Z=62$) M-shell absorption band around 11 Å (1.1 keV) at electron temperatures between 5 and 20 eV. Using point projection absorption spectroscopy, we measured the absolute transmission of an x-ray probe beam through a radiatively heated samarium plasma at different drive temperatures. The measurements show two principal absorption features corresponding to the spin-orbit-split $3d$-$4f$ transitions of Sm IV–Sm X ions. The influence of the heating on the spectral opacity shape was characterized by a shift of the absorption features to higher energy for a hotter plasma. The data are compared with calculations done with the superconfiguration code SCO for different plasma temperatures. The temperature and average ionization inferred from the analysis of the experiment are compared to radiative hydrodynamic simulations. [S1063-651X(98)10201-5]

PACS number(s): 52.25.Nr, 52.25.Jm, 52.50.Jm, 95.30.Ky

I. INTRODUCTION

The measurement and calculation of x-ray absorption in the 100–3000 eV energy range are of great interest for the knowledge of radiative processes occurring in laser-driven inertial confinement fusion [1] or in astrophysics [2]. Many recent experiments for low atomic number elements ($Z<20$) [3–6] and medium-Z elements ($Z\approx 30$) [7–9] have been performed, but only a few measurements have been published for elements heavier than $Z=50$. The absorption of a radiatively heated holmium sample has been measured in the XUV range, showing the $4d$-$4f$ absorption bands [4] at electron temperatures in the range 10–30 eV.

In this paper, we present accurate measurements of the M-shell absorption in samarium ($Z=62$) at around a 11-Å wavelength (1.1-keV photon energy). The parameters of the heating cavity are similar to the one obtained in previous experiments [4,6]. A samarium layer tamped by two carbon layers was heated by the Planckian thermal radiation emitted by a laser-irradiated gold cavity. This radiative drive provides a uniform heating of the sample and insures that the sample is in local thermodynamic equilibrium (LTE) at the time of probing. A statistical approach is necessary to simulate these high-Z absorption features as the atomic complexity limits the efficiency of codes based on detailed configuration accounting (DCA) or detail term accounting for bound-bound and bound-free spectra [10]. Here we used the photoabsorption code SCO to interpret the experiment [11]. The aim of this work was to understand the x-ray absorption of high-Z materials at low temperatures and to evaluate the capability of the SCO code to describe it. In particular, one goal was to estimate the effect of configuration interaction which has been shown to play an increasing role in high-Z elements by redistributing the intensity among the spin-orbit-split nonrelativistic unresolved transition arrays [12].

II. EXPERIMENTAL SETUP AND RESULTS

The samarium sample was heated by the thermal radiation emitted by a 3-mm-diameter laser-heated gold spherical hohlraum. The iodine laser ASTERIX IV at the the Max Planck Institut für Quantenoptik laser facility was used [13]. The main beam delivered up to 250 J in a 400-ps duration pulse at its third harmonic (0.44-μm wavelength), and was focused in the hohlraum. The absorber foil consisted in a self-standing Sm_2O_3 foil (20 μg/cm^2 thick, as ordered from the manufacturer) tamped by two 8-μg/cm^2 carbon foils. The two carbon foils reduced the decompression of the expanding samarium plasma, and provided a quasihomogeneous plasma without large temperature and density gradients. The Sm plasma was expected to be at low temperature and at a density sufficiently high to ensure LTE conditions. The thickness of the absorber foil was optimized to provide a uniform heating in volume, and to obtain an optical depth close to unity. One absorber foil glued on one half of the 1-mm-diameter diagnostic hole was first used. Using only half of the holes (see Fig. 1) enables one to measure the absorbed spectrum and the backlighter source intensity during the same shot. To obtain a higher optical depth while keeping the Sm plasma homogeneous, two samarium samples were glued on half of each diagnostic holes. These

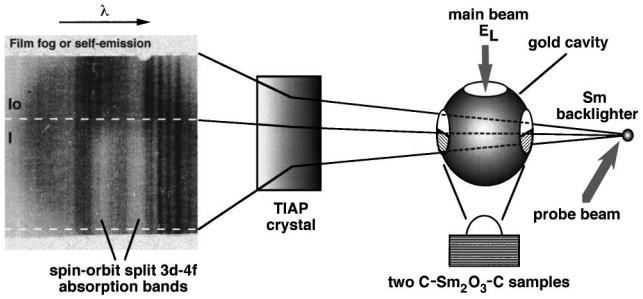

FIG. 1. Schematic drawing of the experiment. The two samples are glued on one half of the two diagnostic holes. Raw film data obtained for 111 J deposited in the hohlraum are used as the sample picture. The source, the transmitted spectra, and the self-emission are measured at different positions on the film, as shown in the figure.

foils were deposited by an evaporation process on a glass substrate from which they were separated by sliding slowly the sample from the substrate in water. The self-standing C-Sm_2O_3-C foils floating on the water surface were then glued onto the diagnostic holes of the target.

The experimental setup is shown in Fig. 1. Point projection spectroscopy method was used to probe the heated sample [14,15]. An x-ray probe beam was created by focusing a second laser beam (50 J, 400 ps at 1.3-μm wavelength) on a samarium foil. The laser intensity was 10^{15} W/cm^2 in an 80-μm full width at half maximum focal spot size. A samarium foil was used for the backlighter (BL) in order to obtain a high continuum emission in the probed spectral range. The BL target was set at a distance of 1 cm from the hohlraum sufficient to avoid heating of the sample by the BL source. The BL x-ray emission pulse duration was 400 ps, and determined the time integration of the measurement. The temporal delay between the peak of the laser pulse irradiating the cavity and the BL laser pulse was 800 ps, i.e., long enough to avoid a large time variation of the Sm temperature and density during the probing time, as can be seen in the plasma simulation shown in Sec. III (Fig. 3).

The BL emission and its transmission through the probed plasma were simultaneously measured by a thallium ammonium phosphate crystal protected by a 10-μm beryllium filter. An aperture was set between the cavity and the spectrograph filter in order to limit the background radiation, and to protect the detector from plasma debris. Data were recorded on Kodak DEF films, calibrated during the experiment by using known step filters. The backlighter emission was spectrally calibrated by recording on the same film a samarium spectrum and a sodium spectrum as a reference. The absolute accuracy in the energy calibration was estimated to be better than 1 eV (10 mÅ), and the spectral resolution was $\lambda/\Delta\lambda \approx 2000$ limited by the backlighter size of 80 μm. The curvature of the lines was corrected. The self-emission coming from the inner walls of the cavity was measured for each laser energy deposition. This emission was found to be negligible when the main laser energy was below 200 J. For higher energy measurements, this emission contribution was measured on the side of the diagnostic hole image on the film, and subtracted from the absorption signal. The two zones in which the BL spectrum I_0 and the transmitted intensity I are measured are apparent in the image obtained for 110 J deposited in the hohlraum (see Fig. 1). All the spectra have been corrected from the film fog. The spectral range was limited to 1.06–1.16 keV by the size of the diagnostic hole.

Figure 2 shows the measured sample transmission. After subtracting the background and the self-emission, the transmission was obtained by dividing the transmitted spectrum by the backlighter source spectrum. The spectra were obtained for different laser intensities in the hohlraum, ranging from 60 to 250 J, as indicated in Fig. 2. The drive temperature corresponding to this deposited energy was interpolated from previous measurements performed under similar conditions [16]. The drive temperatures were respectively 42, 51, 58, and 67 eV for 60-, 111-, 170-, and 250-J laser energies.

Two well separated absorption structures were observed. They correspond to the spin-orbit-split components of the $3d$-$4f$ transitions of samarium. A shift of the $3d$-$4f$ structures to higher energies appears for higher laser intensities due to the increasing Sm ionic charge. Besides the main features, one can note small absorption features at 1.12–1.16 keV for the 60-J shot, which disappear at higher laser intensity. No interpretation has been found to date for these structures.

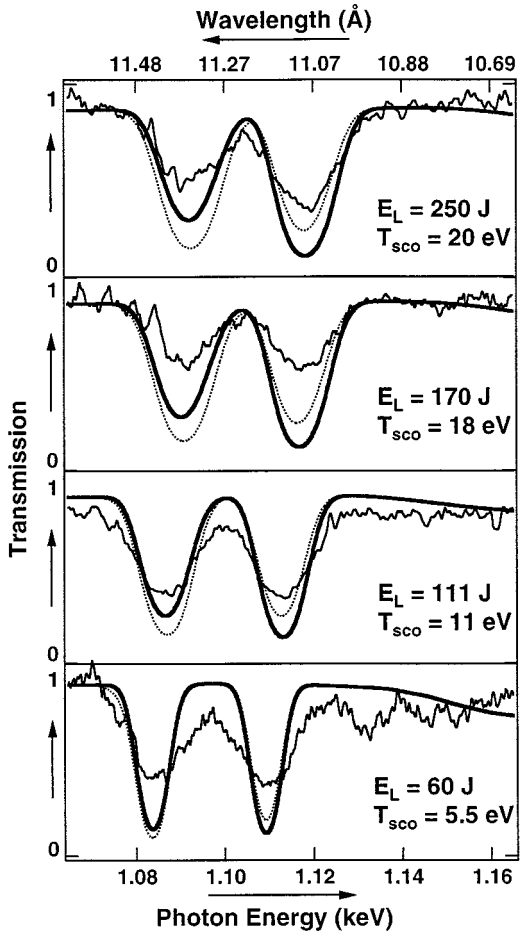

FIG. 2. Absorption spectra of a samarium plasma for different laser energies deposited in the cavity: the plain thin line is the experiment; the heavy plain line is the SCO calculation with configuration interaction; and the dashed line is the SCO calculation without configuration interaction. The laser energy and electron temperature used in the calculation to fit the experiment are indicated.

III. COMPARISON WITH OPACITY MODELING

For a comparison with opacity models, the temperature and density of the C-Sm_2O_3-C sample are needed. For this purpose, hydrodynamic simulations were performed with the MULTI [17] radiative hydrocode, in which a Planckian drive radiation calculated with the experimentally determined radiation temperature [16] was used as an input. The pulse duration of the drive was 0.5 ns. Opacities and emissivities used in MULTI were calculated by a new method based on the modeling of the one-electron atomic potential in the framework of the average atom approach [18]. In this model, collisional-radiative equations of an average ion are solved, and the resulting screened charges are used to reconstruct the one-electron atomic potential. Average atom wave functions,

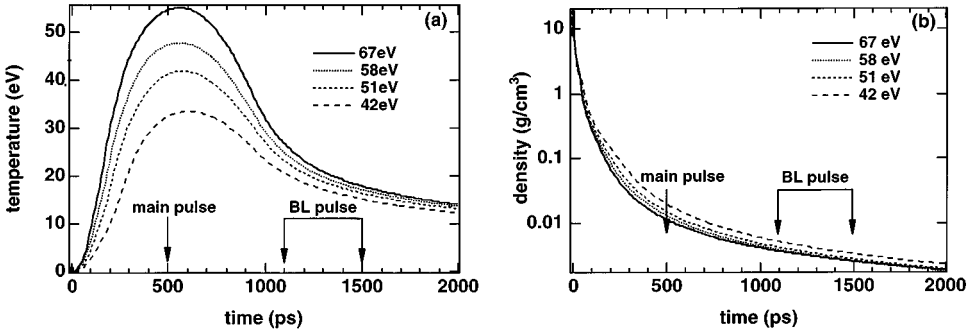

FIG. 3. Electron temperature (a) and matter density (b) calculated with the MULTI hydrocode at the center of the samarium oxide sample as a function of time for drive radiation temperatures corresponding to the four laser energies deposited in the hohlraum. The drive maximum ($t=0.5$ ns) and the probe BL time ($t=1.3\pm0.2$ ns) are indicated in the figure.

oscillator strengths, and Slater integrals are calculated by quantum mechanics in the reconstructed potential. Figure 3 shows the temporal evolution of the electron temperature and the density at the center of the samarium oxide layer as given by MULTI for the four radiation drive temperatures studied. The peak of the x-ray drive and of the probe backlighter pulse are located at 0.5 and 1.3 ± 0.2 ns, as indicated in Fig. 3. During the BL probe, the density of the sample given by MULTI is $(4\pm0.5)\times10^{-3}$ g/cm^3, fairly independent of the drive temperature. The variation of the temperature calculated at the center of the samarium oxide layer and integrated over the temporal duration of the BL pulse is shown in Fig. 5. The temperature and density inhomogeneities due to residual gradients in samarium are below 1 eV and 0.001 g/cm^3, respectively.

The measured transmission spectra obtained in the four shots have been compared to the theoretical spectra from the code SCO developed by Blenski and co-workers [11]. This code calculates photoabsorption in LTE conditions in the superconfiguration approximation proposed by Bar-Shalom and co-workers in the STA code [19]. Superconfigurations are groups of configurations which are close in energy. In this superconfiguration approach, both terms and configurations are treated statistically. In the limit where each superconfiguration contains only one configuration, the superconfiguration approach is identical to the DCA method in which the terms are unresolved and statistically treated. In the case of the $3d$-$4f$ transitions, the orbital relaxation effects are important for the precision of the calculated transition energies, and have been included within the superconfiguration formalism [11]. The differences between the physics of the STA code [19] and the physics of the SCO code were discussed in Ref. [11]. For the purpose of the present comparison, 200 superconfigurations were used in order to calculate the photoabsorption of samarium. The option of the SCO code used here calculates the photoabsorption of mixtures. In this version, an effective density is calculated for each element of the mixture within the Thomas-Fermi approximation from the condition that the free electron densities of the atoms of all elements are equal. Photoabsorption is calculated for each element, and the total spectrum is the mass-weighted sum of the photoabsorption of all constituents.

The transmission was evaluated from the SCO photoabsorption coefficients taking the manufacturer value of 40 (2×20) μg/cm^2 for the areal mass density of the Sm_2O_3 mixture. An experimental spectral resolution of 0.5 eV was assumed, but the convolution with the finite instrument width does not change the shape of the calculated transmission spectra. Indeed, the configuration and term broadening are much larger than the experimental width. We also took into account the absorption from the carbon foils [areal mass density of 32 (4×8) μg/cm^2], but its influence on the calculated spectra was practically negligible. The presence of oxygen mixed with samarium (Sm_2O_3) gives a dilution factor and modifies slightly the continuum absorption.

The results from the SCO code reproduce well the main features of the measured transmission spectra, i.e., the presence of the two spin-orbit-split $3d$-$4f$ transition arrays (SOSA's) [20] averaged over the configurations. According to the statistical character of the superconfiguration method, the detailed features due to terms are smeared out. For each experimental case, the electron temperature of the Sm foils was deduced from the best fit of the the calculated SOSA's with the energy of the experimental spin-orbit-split components as shown in Fig. 2. The density was taken from the MULTI code simulations at the BL time as shown in Fig. 3. The most precise adjustment of the temperature was obtained from a fine adjustment of the positions of the peak of a gaussian fitted on the experimental absorption structures with the two minima of the transmission curves calculated with the SCO code. Results are reported in Table I and Fig. 5. The deduced electron temperature varies from 5.5 to 20 eV for the shots with laser energies between 60 and 250 J. For the three highest energy cases, an excellent agreement was found between the calculated and measured energy difference of

TABLE I. Average ionization $\langle Z\rangle$ at the center of the samarium oxide sample as a function of laser drive energy as given by the comparison of experiment with SCO and given by MULTI. The drive temperature and the experimental foil temperature are reported in the table.

Laser energy (J)	Drive temperature (eV)	T_e Expt.-SCO (eV)	$\langle Z\rangle$ Expt.-SCO	$\langle Z\rangle$ MULTI
60	42	5.5 ± 2	2.7	6.9 ± 0.7
111	51	11 ± 1.5	5.3	7.4 ± 0.8
170	58	18 ± 1	7.9	7.7 ± 1.0
250	67	20 ± 1	9.0	8.0 ± 1.0

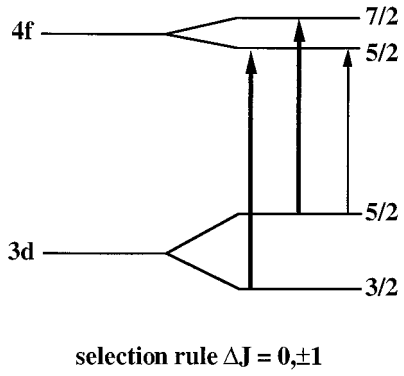

FIG. 4. Energy diagram of the $3d$-$4f$ transitions involved in the main absorption structures. Thick lines show the two strongest $\Delta j = 1$ transitions.

the spin-orbit-split components (see Fig. 2). For the lower energy case, this agreement is not as good. The two components cannot be fitted with the same electron temperature. This gives an uncertainty between 1 and 2 eV in the temperature determination. This could be attributed to the existence of gradients inside the foil for a low drive temperature. A similar uncertainty could also arise from the treatment of the static screening in the thermodynamic model used in the SCO code [11]. Corresponding to these temperatures, the ionization state of the plasma is also predicted by the SCO code for the four experimental cases. The effective charge $\langle Z \rangle$ of the plasma is given in Table I. It shows a large variation of $\langle Z \rangle$ from 2.7 to 9 between 60- and 250-J energy deposited in the hohlraum. The dominant ion in each case is Sm IV, Sm VI, Sm IX, and Sm X.

Figure 2 presents the comparison between the measured transmission spectra and two calculated transmissions: one in pure j-j coupling (i.e., without the configuration interaction), and the second in which the configuration interaction has been included. It has to be noted that the strengths of the two dominant spin-orbit structures seem to be modified by the configuration interaction of the two relativistic subconfigurations belonging to one nonrelativistic configuration. This effect has been discussed in the literature [12,21]. This special case of the configuration interaction can be viewed as a correction to the pure j-j coupling scheme [21]. In the unresolved SOSA corresponding to a one-electron transition between two j-j configurations, only two spin-orbit-split structures can be observed, since the $\Delta j = 0$ transition is much weaker than the two $\Delta j = 1$ transitions (see Fig. 4). In pure j-j splitting, the transition array at the lower transition energy is stronger than the one at higher energy. A redistribution of the oscillator strength from the SOSA at lower transition energy to the SOSA at the higher energy is obtained by taking into account the configuration interaction using the approach proposed by Bauche-Arnoult and coworkers [12,21]. The approach proposed in Ref. [12] can be also applied within the superconfiguration formalism [22]. One observes that the simple effect of the redistribution of the SOSA strength is preserved when the SOSA structures are averaged over configurations. In all shots (with the exception of the one at 170-J laser energy where the two structures are approximately of equal strength) the measured unresolved SOSA structure at higher energy (lower wavelength) shows higher absorption, in agreement with the calculations which include the configuration interaction.

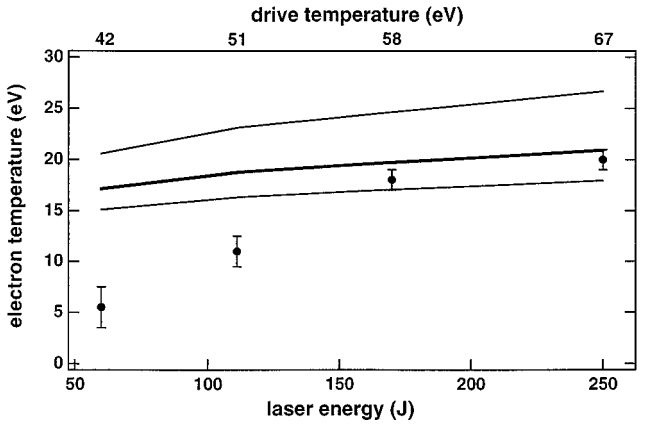

FIG. 5. Calculated electron temperature T_e at the center of the samarium oxide sample as a function of laser drive energy and drive temperature. Plain lines give the temperature as calculated with MULTI. The heavy line gives T_e at the BL peak, i.e., 800 ps after the peak of the laser drive; the two thin lines give T_e at ± 200 ps (corresponding to the BL duration) around this delay. Dots show the temperature deduced from the analysis of the experimental data with the SCO code.

IV. DISCUSSION OF THE RESULTS AND CONCLUSION

The remaining discrepancy between experiment and SCO simulations is that the code gives stronger absorption than the experiment. A possible explanation is that the C-Sm_2O_3-C sample can be deteriorated during the fabrication process. More precisely, while the foil is floating on water, chemical reactions can occur, and the samarium mass could be diminished. The remaining Sm mass could depend on the time the sample remained in water, which can vary slightly from sample to sample. The SCO code has been run with lower Sm mass in order to fit the height of the $3d$-$4f$ absorption structures. A 20 ± 3-μg/cm^2 total areal mass had to be taken for the double foil Sm_2O_3 to fit the four experimental cases, i.e., a factor of 2 lower than the experimental value. Despite the low signal to noise ratio achieved on the continuum measurement, the calculated continuum absorption on the side of the $3d$-$4f$ transitions seemed to be too weak for this value of the areal mass. The very low areal mass and the discrepancy on the continuum make it hard to believe that this is the only reason for the discrepancy on the $3d$-$4f$ absorption. No other reason could be found for this difference in the calculated and measured sample transmission. Improvements in the theory and in foil thickness measurements are required to go further.

The electron temperature T_e deduced from the fit of the experiment with the SCO code are compared in Fig. 5 to the data given by the MULTI hydrodynamic simulation. These are plotted at three times covering the 400-ps time integration window ($t = 1.1$, 1.3, and 1.5 ns). An overall agreement is obtained and the simulation predictions are fairly good for the two highest laser energy cases. The two lower energy experimental cases give lower T_e than given by MULTI. One reason for this discrepancy may be that the radiation diffusion approximation of MULTI is not working well for the thin

samples used in the experiment to obtain an optical thickness around 1. Another reason is that the opacity model in MULTI is too crude to evaluate the absorption of samarium regards to the atomic complexity of the Sm transitions. Also, at very low temperature, it is more difficult to fit the experiment with the SCO code as the spin-orbit energy difference is not well reproduced.

In Table I we compare the effective charge $\langle Z \rangle_{\text{expt-SCO}}$, to the MULTI values. The values deduced from the comparison of the experiment with SCO show a much larger spread than the MULTI data. At low laser energy, the $\langle Z \rangle_{\text{expt-SCO}}$ is lower than the MULTI data following the temperature behavior. It can be noted that in the MULTI calculation the ionization remains around the xenonlike ion Sm IX ($4s^2 4p^6 4d^{10} 5s^2 5p^6$ atomic structure) which has a closed $5p$ shell and is slightly more stable than the other Sm ionic stages.

In conclusion, the $3d$-$4f$ transitions of samarium have been measured for low temperatures (5–20 eV) at a mass density around 4×10^{-3} g/cm^3. Experimental data are fairly well predicted by simulations. In particular, the measured splitting and positions of the components of the $3d$-$4f$ transitions are in good agreement with calculations based on the superconfiguration approximation. This allows an accurate determination of the mean ionization of the Sm plasma. The higher-energy component of the $3d$-$4f$ absorption structure is equal to or stronger than the other component, which proves redistribution of the oscillator strengths of the spin-orbit-split components by configuration interaction. Remaining discrepancies in the overall absorption depth of the $3d$-$4f$ components is not yet well explained, and could be removed by an accurate determination of the areal mass of the absorbing samples and/or improvements of the theory.

ACKNOWLEDGMENTS

The authors want to thank the technical staff at Max-Planck Institut für Quantenoptik, and in particular Walter Fölsner, for target fabrication. Films were digitized in the Centre de Densitométrie of Institut d'Optique at Paris-Sud University. This work was supported by the European Community through the Human Capital and Mobility program (Large scale facility Contract No. ERB-CI-PDCT0083 and network Contract No. ERBCHRXCT930377). One of us, T.B., acknowledges support from the Centre d'Etudes de Limeil-Valenton.

[1] J. Lindl, Phys. Plasmas **2**, 3933 (1995); E. Storm, J. Fusion Energy **7**, 131 (1988).

[2] F. J. Rogers and C. A. Iglesias, Science **263**, 50 (1994); C. A. Iglesias, B. G. Wilson, F. J. Rogers, W. H. Goldstein, A. Bar-Shalom, and J. Oreg, Astrophys. J. **445**, 855 (1995).

[3] J. F. Seely, U. Feldman, C. M. Brown, B. A. Hammel, C. A. Back, E. Hsieh, and R. W. Lee, J. Quant. Spectrosc. Radiat. Transf. **51**, 349 (1994).

[4] G. Winhart, K. Eidmann, C. A. Iglesias, A. Bar-Shalom, E. Minguez, A. Rickert, and S. Rose, J. Quant. Spectrosc. Radiat. Transf. **54**, 437 (1995); G. Winhart, K. Eidmann, C. A. Iglesias, and A. Bar-Shalom, Phys. Rev. E **53**, R1332 (1996).

[5] J. A. Koch, C. A. Back, C. A. Iglesias, D. L. Williams, R. C. Cauble, E. J. Hsieh, H. N. Kornblum, N. C. Woolsey, J. C. Moreno, A. Asfaw, J. K. Nash, F. J. Rogers, and R. W. Lee, J. Quant. Spectrosc. Radiat. Transf. **54**, 227 (1995).

[6] H. Merdji, K. Eidmann, C. Chenais-Popovics, G. Winhart, J. C. Gauthier, A. Mirone, and C. A. Iglesias, J. Quant. Spectrosc. Radiat. Transf. (to be published).

[7] T. S. Perry, K. S. Budil, R. Cauble, R. A. Ward, D. R. Bach, C. A. Iglesias, B. G. Wilson, J. K. Nash, C. C. Smith, J. M. Forster, S. J. Davidson, F. J. D. Serduke, J. D. Kilkenny, and R. W. Lee, J. Quant. Spectrosc. Radiat. Transf. **54**, 317 (1995).

[8] S. Gary, J. Bruneau, A. Decoster, D. Desenne, F. Garaude, J. P. LeBreton, J. C. Gauthier, J. Bauche, C. Bauche-Arnoult, J. L. Ocana, C. Molpeceres, and M. L. Gamez, J. Quant. Spectrosc. Radiat. Transf. **54**, 155 (1995).

[9] J. M. Foster, D. J. Hoarty, C. C. Smith, P. A. Rosen, S. J. Davidson, S. J. Rose, T. S. Perry, and J. D. Serduke, Phys. Rev. Lett. **67**, 3255 (1991).

[10] C. A. Iglesias and F. J. Rogers, Astrophys. J. **464**, 943 (1996); F. J. Rogers and C. A. Iglesias, Astrophys. J. Suppl. **79**, 507 (1992), and references therein.

[11] T. Blenski, A. Grimaldi, and F. Perrot, Phys. Rev. E **55**, R4889 (1997).

[12] C. Bauche-Arnoult, J. Bauche, and M. Klapisch, J. Phys. B **24**, 1 (1991).

[13] H. Banmhucker, G. Brederlow, E. Fill, R. Volk, S. Witkowski, and K. Y. Witte, Appl. Phys. B: Photophys. Laser Chem. **61**, 325 (1995).

[14] C. L. S. Lewis and J. McGlinchey, Opt. Commun. **53**, 179 (1985).

[15] J. M. Foster, Rev. Sci. Instrum. **59**, 1849 (1988).

[16] G. Winhart, Ph.D. thesis, Max Planck Institut für Quantenoptik, 1996.

[17] R. Ramis, R. F. Schmalz, and J. Meyer-ter-Vehn, Comput. Phys. Commun. **49**, 475 (1988).

[18] A. Mirone, J. C. Gauthier, F. Gilleron, and C. Chenais-Popovics, J. Quant. Spectrosc. Radiat. Transf. (to be published).

[19] A. Bar-Shalom, J. Oreg, W. H. Goldstein, D. Shvarts, and A. Zigler, Phys. Rev. A **40**, 3183 (1989); J. Oreg, A. Bar-Shalom, and M. Klapisch, Phys. Rev. E **55**, 5874 (1997), and references therein.

[20] J. Bauche, C. Bauche-Arnoult, and M. Klapisch, Adv. At. Mol. Phys. **23**, 131 (1988).

[21] J. Bauche, C. Bauche-Arnoult, M. Klapisch, P. Mandelbaum, and J. L. Schwob, J. Phys. B **20**, 1447 (1987).

[22] A. Bar-Shalom, J. Oreg, and W. H. Goldstein, J. Quant. Spectrosc. Radiat. Transf. **51**, 27 (1994).